

# CHARACTERIZATION OF NON-STATIONARY STRUCTURAL NON-UNIFORMITIES IN PAPER

*Markku Kellomäki,<sup>1</sup> Joel J. Pawlak, Yong-Joo Sung  
and D. Steven Keller*

Empire State Paper Research Institute, Faculty of Paper Science  
and Engineering

State University of New York College of Environmental Science  
and Forestry, Syracuse, New York, 13210

<sup>1</sup>Permanent Address: VTT Energy, P. O. Box 1603, Jyväskylä,  
Finland, FIN-40101

## ABSTRACT

In this investigation, a novel approach to separating the static and stochastic components of paper variability data, such as mass formation or apparent density, was developed. Based on a discrete implementation of the continuous wavelet transform, the method provides information about the scale of features, e. g. flocs or streaks, as function of position within the data array in one direction. A non-rigorous, yet self-contained theoretical development of the method was given. The main discovery in this work was to mathematically show that, under conditions applying to a typical paper variability data, the distribution of energy among wavelets of different scale and at different positions, or simply, the *local energy map*, can be decomposed into two different parts that contain all the energy related to the *static mean grammage profile* or the *local stochastic variability*.

In order to validate the approach and to justify its value, a set of simulated basis weight maps with different types of streaks were generated and analyzed successfully. This method was even

able to decompose overlapping grammage and formation streaks, which would have been impossible using traditional methods. As a final demonstration, data measured from real papers made in the laboratory and with a pilot machine were analyzed. Apparent density maps were determined using  $\beta$ -radiographic transmission imaging for mass formation and two-sided laser profilometry for local thickness maps. The method was able to reveal floc size variations buried into strong grammage streaks. The periodicity and the scale of the grammage streaks were also characterized by the decomposition of the wavelet map.

## INTRODUCTION

The quality of paper depends heavily on the uniformity of material distribution, within the plane of the sheet and also through its thickness. The heterogeneous pore structure ( $<1\mu\text{m}$ ) substantially influences the absorption of inks and fountain solutions in printing. However, small-scale variations in grammage from about 0.1 mm to 100 mm, referred to as mass formation [1], can have a significant impact on the print quality [2–5], coating uniformity [6], optical [7, 8] and mechanical properties [9]. The stochastic nature of the fiber distribution within the sheet is well recognized [10]. The fibers may exhibit an increased tendency to cluster together and increased flocculation as compared to that found in a random distribution of fibers depending on fiber dimensions [11, 12] forming conditions [12–14] and wet end chemistry [15]. Numerous investigators have developed methods to measure [16–19] analyze [10, 20–23], and model [24, 25] the manner in which fibers are distributed in the final sheet. The uniformity of the fibrous structure may be further degraded by variability in the papermaking process. For example, deterministic variability in machine direction (CD) grammage may result from paper machine vibration or non-uniform stock supply [26, 27]. Non-uniformity in the cross machine direction (CD) may occur at large scales, as for edge effects due to pressure imbalances in the headbox or shrinkage in the dryer section, or at small scales such as uneven slice opening or the turbulent flows in the headbox and forming zone [28]. Thus, the formation of paper is dependent on a variety of factors that determine the size distribution and intensity of features over a broad range of scale, in regular or random spatial distributions. To examine the statistically non-stationary nature of machine made papers, methods are necessary to identify characteristic scales for these factors.

Cross machine non-uniformities with relatively high persistency in the machine direction are referred to as “streaks”. The occurrence of streaks is a serious concern for product quality from lightweight papers to board grades. Streaks may be regularly or randomly distributed across the CD. Their position may be essentially fixed (static), or they may be unstable and vary in cross machine position as the sheet is examined at different locations in the MD. Streaks are not limited to variations in grammage, but may also appear as variations in floc size distribution (formation), mean fiber orientation [29, 30], filler or moisture content, thickness, surface roughness or even Z-directional tensile strength [31]. While on-machine [32] and off-machine [33] instruments are available to detect and characterize cross machine variability, more rigorous methods are needed in order to obtain a thorough decomposition of the contributions from the various sources that contribute to the overall structure. This investigation applied a recently introduced approach, the *wavelet technique*, for use in distinguishing the local spectral characteristics, i. e., *simultaneous scale and space analysis*, of mass formation and local apparent density of paper.

Keller et al. [34,35] introduced an analytical method based on one-dimensional continuous wavelet transform to examine the spectral-spatial relationship for paper variability data. The method was demonstrated using trigonometric functions. It was validated by applying the technique to a series of simulated images representing variations in grammage, flocculation, gradient flocculation and mean fiber orientation. To establish a frame of reference, samples were extensively characterized by conventional statistical, formation and spectral analyses. The continuous wavelet analysis developed in that investigation calculated spectral density in the same units as the formation (wavelength) spectrum of Norman and Wahren [23], while extending it to include the spatial domain. The simultaneous scale-space representation of the wavelet transform exhibited a lower spectral resolution as compared to the power spectra derived from the Fourier transform. The wavelet analysis also showed a susceptibility to individual features, which tended to confound simple interpretation of singular local energy maps. However, a solution was developed whereby wavelet spectral maps, determined from parallel lines within the image were consolidated, so that local scale features in a non-stationary image could be characterized.

Bouydain et al. [36] reported the use of discrete wavelet transforms to conduct multiresolution analysis [37] on light formation images of paper. That approach generates two-dimensional decompositions of the floc pattern into a series of band-passed images of increasing resolution. The result is quite similar to the earlier works of Johansson [38] and MacGregor et al. [39]. The structure is characterized by further analysis of the individual band-pass

images, even into representative parameters, e. g., *wavelet formation indices* [36]. The approach of Keller et al. [34] used in this study, differs significantly from these techniques in that a one-dimensional analysis is used to characterize features that are statistically non-stationarity in one direction. The mathematical and practical differences have been detailed previously [34].

While formation measurement, both mass and light, have been a vital part of the investigation of in-plane paper structure, it is well recognized that local apparent density may be more directly related to certain paper properties, such as porosity, sorption, flexural stiffness or even internal bonding. The inability to directly correlate light and mass formation of calendered sheets [40–42] results from the non-uniformity of apparent density and local light scattering properties. Regions of higher density (lower porosity) are expected to have different liquid absorption behavior as compared to lower density regions. Accurate measurement of apparent density has eluded the paper scientist due to the difficulty in measuring the local thickness in a manner that is accurate and non-invasive. The introduction of a method for fine scale mapping of thickness based on opposing displacement transducers, referred to as opposing spherical platens, [43,44] enabled the mapping of local apparent density when coupled with mass formation imaging [45]. While the utility of this approach was evident, the spatial resolution was limited and the platens contacted the surface, which imparted a small but finite deformation.

Contemporary methods for measuring local apparent density make use of noncontacting laser profilometers based on either the dynamic focusing [46] or triangulation [47] to determine local thickness. Laser range sensors are held in opposition with the sample in between so that the roughness data from both sides of the sheet are measured simultaneously. The sensors are raster scanned in the plane of the sample so that an areal map is obtained. Oba [48] used a thickness method based on a dynamic focusing range sensor [49] to study the statistics of local apparent density variation. A method based on laser range triangulation was used in this investigation to measure local thickness and map the local apparent density.

The objective of this study was to explore the use of spectral analysis of mass formation and local apparent density images to distinguish between stable and stochastic streaking patterns within machine made papers. Specifically this involves the use of a continuous wavelet transform to obtain spectral energy maps of the data sets, from which novel analytical methods were be used to make the distinction. Validation of all methods was attained by analyzing simulated images where local mean grammage, variance of grammage, and scale of flocs is controlled as a function of position in a single (CD) direction. Laboratory and machine made papers that had notable streak defects were tested in order to demonstrate the viability of the method.

## **THEORETICAL APPROACH**

Numerous investigators have analyzed the deterministic [50,51] and stochastic [27,52,53] nature of paper using power spectral analysis based on Fourier transformation of one- and two-dimensional [54] data sets. In Fourier transformation, the analyzed function is decomposed into a sum of trigonometric functions. As trigonometric functions are perfectly localized in the frequency domain, they spread infinitely in spatial domain. This form of analyzing functions is well suited for detecting periodicities in the data, which are already known to have characteristic frequencies. If the analyzed function is not periodic (e. g., a single pulse), an infinite number of analyzing functions are needed to reconstruct it. This makes Fourier analysis, at least in its basic formulation, rather inefficient for analyzing spatially localized defects, as in the present case of streaks. Wavelet transform analysis has the capability to overcome these limitations. In this section a brief, non-rigorous introduction into the mathematical background of the continuous wavelet transform will be provided. More detailed presentations can be found in various articles [55–57] by other authors and our previous publications [34,35].

### **Analyzing Functions**

Considering the problems of Fourier analysis in non-periodic cases, it is intuitively evident that the use of a set of pulse-like analyzing functions, localized both in spatial and frequency domains, would perform better. Wavelet transform analysis is based on this concept. The set of analyzing functions is called a wavelet family. Consider the one-dimensional case in which such a family of functions,  $\psi_{a,b}(x)$  can be generated by

$$\psi_{a,b}(x) = |a|^{-1/2} \psi\left(\frac{x-b}{a}\right), \quad a, b \in \Re, a \neq 0, \quad (1)$$

where  $\psi$  is called the mother wavelet,  $a$  is the scale of the wavelet (spatial width) and  $b$  is the position (center) of the wavelet. From Equation 1 one finds that a family of wavelets may be generated by different spatial dilations, compressions, and translations of the mother wavelet  $\psi(x)$ .

There are a few restrictions [55] on the choice of the mother wavelet: admissibility, similarity of the function in dilation and translation, invertibility of the transform, and regularity, in which the function has localization in the physical and Fourier domain. The admissibility condition requires the basic wavelet to satisfy the relation

$$C_\psi = 2\pi \int_{-\infty}^{\infty} |\hat{\psi}(k)|^2 \frac{dk}{|k|} < \infty, \quad \text{where } \hat{\psi}(k) = \frac{1}{2\pi} \int_{-\infty}^{\infty} \psi(x)e^{-ikx} dx, \quad (2)$$

where  $C_\psi$  is called the admissibility constant. Integrability of  $\psi(x)$  together with Equation 2 implies that it has mean of zero. Therefore, in a wavelet transform the *local* DC-component (local mean value of the data) is eliminated.

Let us take a look at the Mexican hat or Marr wavelet, which we have used in our previous publications [34,35], and in this study as the mother wavelet:

$$\psi^{G2}(x) = (x^2 - 1) e^{-x^2/2} \quad (3)$$

This choice of the mother wavelet has been very popular in analyzing turbulent flow and other aspects of fluid mechanics [57–61]. Figure 1a shows wavelets of family  $\psi^{G2}_{a,b}(x)$  with different values of scale  $a$ . In Figure 1b, different values of position  $b$  are illustrated. The Mexican hat family of wavelets is particularly suitable for finding local extrema of the data such as floes, voids or streaks in grammage maps of paper [35].

The wavelength of a cosine and the scale of the Mexican hat wavelet have been shown to be related as

$$\lambda = a \frac{2\pi}{\sqrt{2.5}}. \quad (4)$$

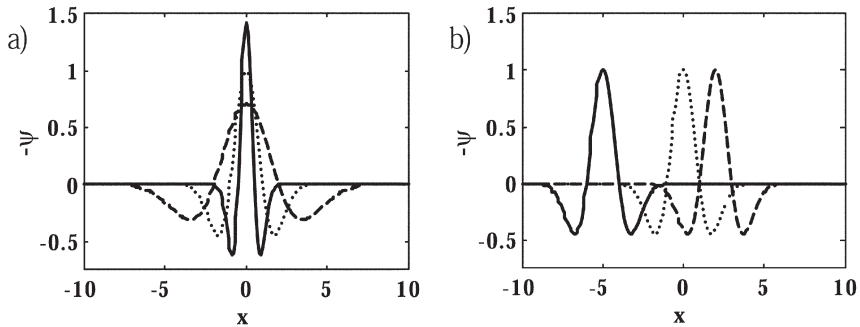


**Figure 1** Family of wavelets  $\psi^{G2}_{a,b}(x)$  for: a) where the position factor  $a = 0.5, 1.0, 2.0$  (solid, dotted and dashed line, respectively, and  $b = 0.0$ ); and b) where the dilation factor  $b = -5.0, 0.0$  and  $2.0$  (solid, dotted and dashed line, respectively, and  $a = 1.0$ ).

Due to the familiarity of wavelength representation, we will use it to plot the wavelet results in the following sections.

### Continuous Wavelet Transform

Continuous wavelet transform is defined as an inner product between function and basis functions (similar to Fourier transform):

$$\tilde{f}(a, b) = \int_{-\infty}^{\infty} f(x) \psi_{a,b}^*(x) dx = \langle f, \psi_{a,b} \rangle, \quad (5)$$

where wavelet coefficients  $\tilde{f}(a, b)$  indicate the similarity (correlation) of  $f(x)$  and  $\psi_{a,b}(x)$  as a function of both scale (wavelength) and position. Wavelet transform thus gives a two-dimensional result from the analysis of a one-dimensional data, whereas Fourier transform gives only one-dimensional (scale) information. Energy is conserved in wavelet transform:

$$E = \int_{-\infty}^{\infty} |f(x)|^2 dx = C_{\psi}^{-1} \int_{-\infty}^{\infty} \int_0^{\infty} |\tilde{f}(a,b)|^2 \frac{da db}{a^2}, \quad (6)$$

where  $C_{\psi}^{-1}$  is given by Equation 2. Local energy density  $\rho(a,b)$  is defined by:

$$\rho(a,b) da db = C_{\psi}^{-1} |\tilde{f}(a,b)|^2 \frac{da db}{a^2}. \quad (7)$$

It can be interpreted as a “power spectrum” at position  $b$  as a function of scale  $a$ . Comparing Equations 6 and 7 we notice that  $\rho(a,b) da db$  is identified as *local variance* of scale band  $[a, a + da)$  at position interval  $[b, b + db)$ .

### Numerical Implementation

By applying generalized Parseval’s theorem, the Fourier transform of Equation 3 it is straightforward to show [55] that

$$\tilde{f}(a,b) = a^{1/2} F^{-1}(\hat{f}(k) \hat{\psi}^*(ka))(b), \quad (8)$$

where  $F^{-1}$  denotes inverse Fourier transform,  $\hat{f}(k)$  is Fourier transform of function and  $\hat{\psi}(k)$  Fourier transform of mother wavelet. The tedious convolution integral, cf. Equation 5, can be thus computed more efficiently in Fourier domain. In a discrete implementation there is an additional benefit: small-scale wavelets are more accurately represented in wavenumber space than in spatial representation.

## Analysis of Two-Dimensional Data

If we are interested in average one-dimensional properties, e. g. into  $x$  direction, of a two-dimensional data matrix  $f_i(x)$ , we can compute local energy maps of each row of the matrix and average them. The mean energy map  $\langle \rho(a,b) \rangle$  is called *the composite local energy density (CLE)*, defined as:

$$\langle \rho(a,b) \rangle da db = \frac{C_w^{-1}}{a^2} \frac{1}{N} \left( \sum_{i=1}^N |\tilde{f}_i(a,b)|^2 \right) da db = dC_{ab} = \frac{C_w^{-1}}{a^2} \langle |\tilde{f}_i(a,b)|^2 \rangle da db, \quad (9)$$

where  $N$  is the number of rows of the matrix.

## Decomposition of CLE into Static and Stochastic Components

From the perspective of scale analysis, each line of a stochastic two-dimensional data matrix (such as grammage map), can be considered as a sum of a static profile and stochastic variation. Let us define

$$h(x) := \langle f_i(x) \rangle, \quad (10)$$

where  $f_i(x)$  is the  $i$ th row of the data matrix, and  $\langle \rangle$  means averaging over the rows.

Now we can write

$$f_i(x) = h(x) + g_i(x), \quad (11)$$

where  $h(x)$  is the static profile, and  $g_i(x)$  is the stochastic signal whose scale variations we are interested in determining. From Equations 10 and 11 we find that  $\langle g_i(x) \rangle = 0$ . The mean total energy of the matrix is

$$\langle E_i \rangle = \left\langle \int_{-\infty}^{\infty} |f_i(x)|^2 dx \right\rangle = \int_{-\infty}^{\infty} \langle f_i^2(x) \rangle dx, \quad (12)$$

because  $f_i(x) \in \Re$  and  $f_i^2(x) \geq 0$ . The integrand can be written as

$$\begin{aligned} \langle f_i^2(x) \rangle &= \langle h^2(x) + 2h(x)g_i(x) + g_i^2(x) \rangle = h^2(x) + 2h(x)\langle g_i(x) \rangle + \langle g_i^2(x) \rangle \\ &= h^2(x) + \langle g_i^2(x) \rangle. \end{aligned} \quad (13)$$

Using Equations 6, 10 and 13 and the fact that  $g_i^2(x) \geq 0$  we can write Equation 12 as

$$\begin{aligned}
 \langle E_i \rangle &= \int_{-\infty}^{\infty} h^2(x) dx + \int_{-\infty}^{\infty} \langle g_i^2(x) \rangle dx \\
 &= C_{\psi}^{-1} \int_{-\infty}^{\infty} \int_0^{\infty} |\tilde{h}(a,b)|^2 \frac{da db}{a^2} + C_{\psi}^{-1} \int_{-\infty}^{\infty} \int_0^{\infty} \langle |\tilde{g}_i(a,b)|^2 \rangle \frac{da db}{a^2} \\
 &= C_{\psi}^{-1} \int_{-\infty}^{\infty} \int_0^{\infty} (|\langle \tilde{f}_i \rangle(a,b)|^2 + \langle |\tilde{g}_i(a,b)|^2 \rangle) \frac{da db}{a^2} \quad (14)
 \end{aligned}$$

Comparing Equations 9 and 14 we find that

$$\langle \rho(a,b) \rangle = \frac{C_{\psi}^{-1}}{a^2} (|\langle \tilde{f}_i \rangle(a,b)|^2) + \frac{C_{\psi}^{-1}}{a^2} (\langle |\tilde{g}_i(a,b)|^2 \rangle) =: \rho_h(a,b) + \langle \rho_g(a,b) \rangle. \quad (15)$$

It was thus shown that the composite local energy density *decomposes* into parts related to the *static mean profile* and to the *stochastic local variation*. When we are interested in local variation, we would prefer to study the *composite stochastic local energy density* (CSLE)  $\langle \rho_g(a,b) \rangle$  rather than  $\langle \rho(a,b) \rangle$ .

If the data matrix is a result of a random deposition process, as in the case of paper [10, 62] the variances  $\sigma^2(x)$  (or energies) of all scales are all proportional to the number  $N(x)$  of deposited objects, i.e. fibers or flocs. On the other hand,  $\langle f_i(x) \rangle$  is proportional to  $N(x)$ . Therefore, one can more easily visualize coherent scale structures by studying the *composite normalized stochastic local energy density* (CNSLE) given by

$$\langle \rho_g^N(a,b) \rangle = \frac{\langle \rho_g(a,b) \rangle}{\langle f_i(b) \rangle} = \frac{1}{\langle f_i(b) \rangle} \frac{C_{\psi}^{-1}}{a^2} (\langle |\tilde{f}_i(a,b)|^2 \rangle - |\langle \tilde{f}_i \rangle(a,b)|^2). \quad (16)$$

Looking at the units of this expression one finds that it is equivalent to the formation number defined in [53]. For practical plotting purposes (color proportional to energy rather than energy density) one defines the *composite local energy* (CLE) map from earlier work of Keller et al. [34, 35] as  $\langle \rho(a,b) \rangle da db$ ; the *composite normalized stochastic local energy* (CNS-LE) map as  $\langle \rho_g^N(a,b) \rangle da db$ ; and the *static mean profile local energy* (SMP-LE) map as  $\rho_h(a,b) da db$ .

## **EXPERIMENTAL**

### **Materials**

Hand sheets with imposed non-uniformity of flocculation, to imitate streaking, were prepared using a modification of the TAPPI standard method T-205. An apparatus was constructed to divide the volume of a standard British handsheet mold into three sections using two parallel baffles positioned vertically. By treating the fibrous suspension differently in the center section, as compared to the two outer sections, handsheets with distinct strips with controlled non-uniformity could be made. To obtain a handsheet with a strip of higher or lower grammage in the center, greater or lesser amounts of fibrous suspension were added to the center section. A strip with different formation (flocciness) was generated by agitating the center and the outer sections to a greater or lesser extent. Both procedures were combined to obtain handsheet samples with strips with different grammage and formation. Handsheets were composed of unbeaten, bleached softwood kraft (BSWK).

The machine made samples were supplied by a company that generated the sample on a pilot paper machine under conditions that created streaking. The samples were made of bleached softwood kraft with no filler and had a mean grammage of 42 g/m<sup>2</sup>.

### **Formation Measurement**

The grammage maps for the handsheet and machine made paper samples were determined using  $\beta$ -radiographic imaging using the procedure described by Keller and Pawlak [63]. In this method, the paper sample was held in compression between a <sup>14</sup>C radiation source with spatially uniform activity and a photostimulable storage phosphor screen. Following exposure, the storage phosphor screen was digitized using a PhosphorImagerSI™ scanning instrument manufactured by Molecular Dynamics (Sunnyvale, CA). The radioactive source consisted of a 102 mm × 102 mm × 1 mm PMMA film labeled with <sup>14</sup>C (Amersham Co., UK) with a total activity of 6.17 mCi. The surface activity of the source was determined to be 11.8 ± 0.1 mCi/m<sup>2</sup> by calibrating with an NBS traceable <sup>14</sup>C reference source #1692, NES-264 (NEN Products, Dupont). The source was affixed to the flexible backing of an exposure cassette supplied with the storage phosphor instrument.

At the end of the exposure period, screens were transferred directly to the PhosphorImager for development and digitization. The screens were scanned at a 100 μm pixel size in this investigation. The instrument was calibrated to convert gray levels to grammage using a Mylar step wedge. The storage phosphor system had a linear response to beta ray exposure that

spanned more than three orders of magnitude, which made it quite sensitive  $\sim 0.1 \text{ g/m}^2$ .

Spatial uniformity of the source / screen combination was determined to be within about 3% across the 100 mm span. Spatial uniformity is critical for the streak analysis proposed in this study. Correction of spatial non-uniformity, as may be necessary for camera scanning of X-ray film [18, 64] by using corrective masks, may correct the intensity of the grammage profile, but will also affect the contrast so that a variation in the floc contrast will also be affected. This results in an unwanted artifact that may be interpreted as part of the paper structure. The use of a spatially uniform source and imaging system is essential.

### **Local Thickness Measurement**

The local thickness of paper samples was mapped using an instrument based on two sided, laser profilometry. The paper was held between two range sensors held in opposition, while scanning both sides simultaneously. The laser range sensors (DRS-300, Cybermetrics Corp., Minneapolis, MN) detect distance to the surface using triangulation of the laser beam at a  $35^\circ$  incident and  $35^\circ$  reflected angle. The sensors have a detection limit of  $0.35 \mu\text{m}$ , and an operating resolution of  $1 \mu\text{m}$ . Beam spot size is nominally  $20 \mu\text{m}$ . To accommodate severe out of plane deformation of the sample, the coarse scale range of both laser sensors was adjusted using positioning stages. Local thickness was measured pointwise over a region of the sample by moving the range sensors in a raster pattern across the in-plane area of the sample using positioning stages with  $1 \mu\text{m}$  resolution over a 6-inch range. The instrument was isolated from vibrations using an optical table, and air currents in an environmental chamber where Tappi Standard conditions were held for the duration of the test. Control of the laser and positioning stages, and data acquisition was conducted using a computer workstation. In addition to mapping the local thickness, the out of plane deformation of the centerline of the paper, referred to as the *mean out of plane deformation*, was also mapped.

### **Local Apparent Density**

Local apparent density was determined by reducing the grammage by the thickness, pointwise over the area of measurement, i.e.,  $50 \text{ mm} \times 50 \text{ mm}$ . The samples were marked with registration points and imaged to obtain a grammage map with a  $100 \mu\text{m}$  pixel size. After thickness was mapped to the same resolution, a digital algorithm registered images and the calculation of local apparent density was performed.

## GENERATION OF SIMULATED FLOCCULATED GRAMMAGE MAPS

In order to study streaks in paper, a natural starting point is to use totally controlled samples generated by computer simulation. Our simulation model generates a two-dimensional, discrete grammage map by depositing individual fibers on a continuous plane and then projecting these fibers to a discrete matrix of arbitrary resolution (element size). This enables us to study the effect of different apertures of formation measurements. In this work the element size was always 100  $\mu\text{m}$ . Fibers, whose dimensions and coarseness can be set to represent real fibers, are deposited randomly according to a preset state of flocculation and orientation. The fibers are assumed to be uniformly rectangular with length,  $l$ , and width,  $w$ . Mean fiber orientation angle  $\theta$  of fibers can have any real value between 0 and  $\pi$ . In Figure 2 we show a close-up of a few fibers projected on a discrete matrix.

Formation is controlled by floc size in our model. Flocs of different size are generated by depositing fibers inside elliptical areas referred to as *elementary flocs*. These elementary flocs that are the target of deposition are already randomly distributed on the plane before fiber deposition. Floc size is controlled by the primary,  $a$ , and secondary,  $b$  axes of these ellipses. In Figure 2b we show some elementary flocs into which the fibers have been deposited. These have close resemblance to flocs that may be found in fiber suspensions.

When realistic grammages are simulated, there are a very large number of flocs to be deposited, e.g., for 10 cm square area generated at grammages of the order of 80  $\text{g/m}^2$  there are millions of fibers. While the examples of networks shown in Figure 2 appears to be very sparse, more realistic-looking grammage maps are generated from depositions of realistic numbers of fibers. In Figure 3 we show three different grammage maps with mean grammage of 40  $\text{g/m}^2$ . The first one, Figure 3a, represents a uniformly random network that may correspond to a laboratory prepared handsheet. The cases shown in Figure 3b and 3c correspond to elementary floc sizes of  $l/2$  and  $l$ , respectively. The changing state of flocculation is evident.

### Control of Formation and Grammage in CD

In the earlier work by Keller et al. [35] a method for generating gradients of flocculation within simulated sheets was established. Expanding on this concept to more closely approximate real systems, we now enable grammage and floc size to be controlled independently using target profiles that are given by

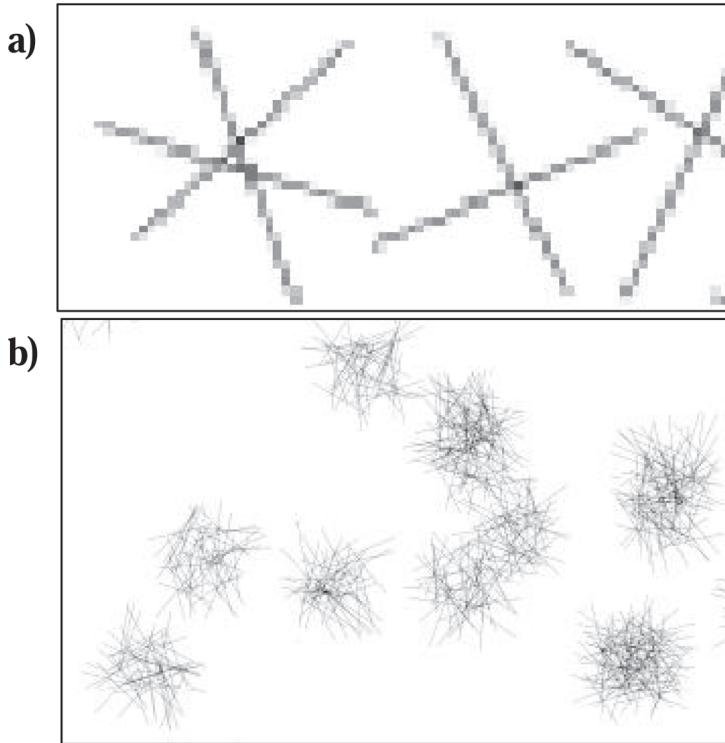


**Figure 2** Projection of a) individual fibers onto a discrete matrix, and b) some elementary flocs with fibers deposited in them.

arbitrary functions of CD position. Also, a gradient in fiber concentration across flocs is introduced, allowing us to control the density profile of the flocs. These tunable profiles give us tremendous possibilities for simulation of different types of streaks. Figure 4 shows an example of the profiles used to generate streaks. The grammage profile was set by the relative probability  $g(x)$  for floc deposition. From Figure 4a we observe that there was one grammage streak to be created at position  $x = 50$  mm with grammage that was 75% of the grammage outside the streak. The floc diameter profile  $d(x)$  shows that there was one floc size streak at position  $x = 145$  mm. In the streak  $d = 3.3$  mm and outside the streak  $d = 6.6$  mm. These flocs were generated to have the same density, i. e., the number of fibers per floc  $n(x)$  was chosen to be proportional to the area (proportional to  $d^2(x)$ ) of the floc. Figure 4b

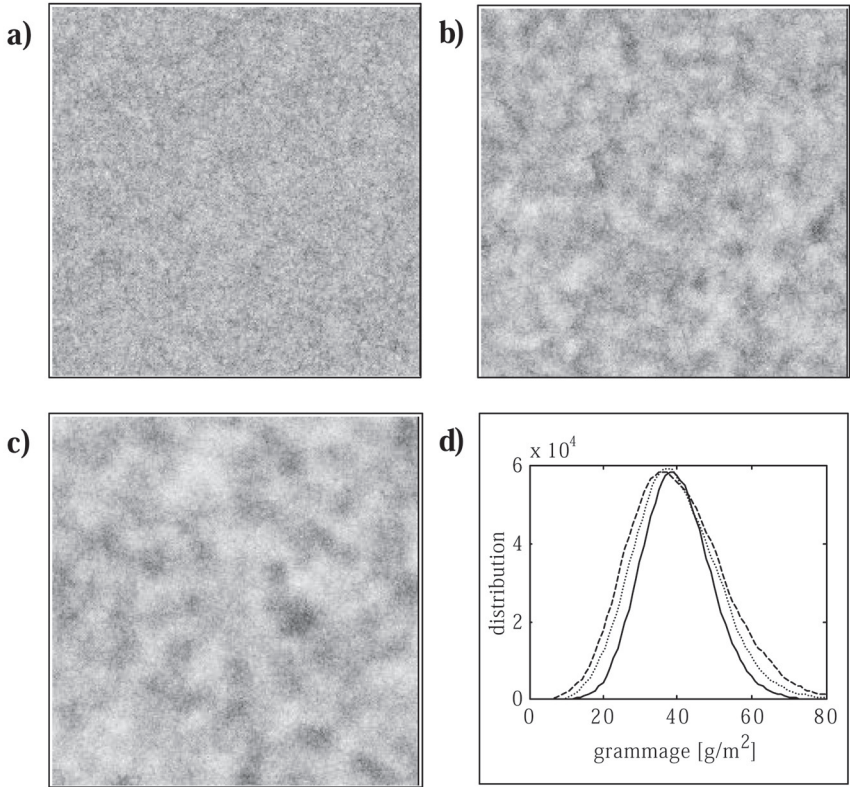


**Figure 3** Different formations with mean grammage  $40 \text{ g/m}^2$  a) random sheet; b) elementary floc diameter  $l_f / 2$  ; c) elementary floc diameter  $l_f$  ; d) Grammage distributions for images a), b) and c) (solid, dotted, dashed, respectively).

shows the generated flocculated fiber network sample at an early ( $4 \text{ g/m}^2$ ) phase of floc deposition, which clearly illustrates how different kinds of flocs start to aggregate at different CD positions according to the target profiles  $g(x)$ ,  $d(x)$  and  $n(x)$ . The mean and standard deviation profiles of grammage of the final sample ( $40 \text{ g/m}^2$ ) are shown in Figure 4c.

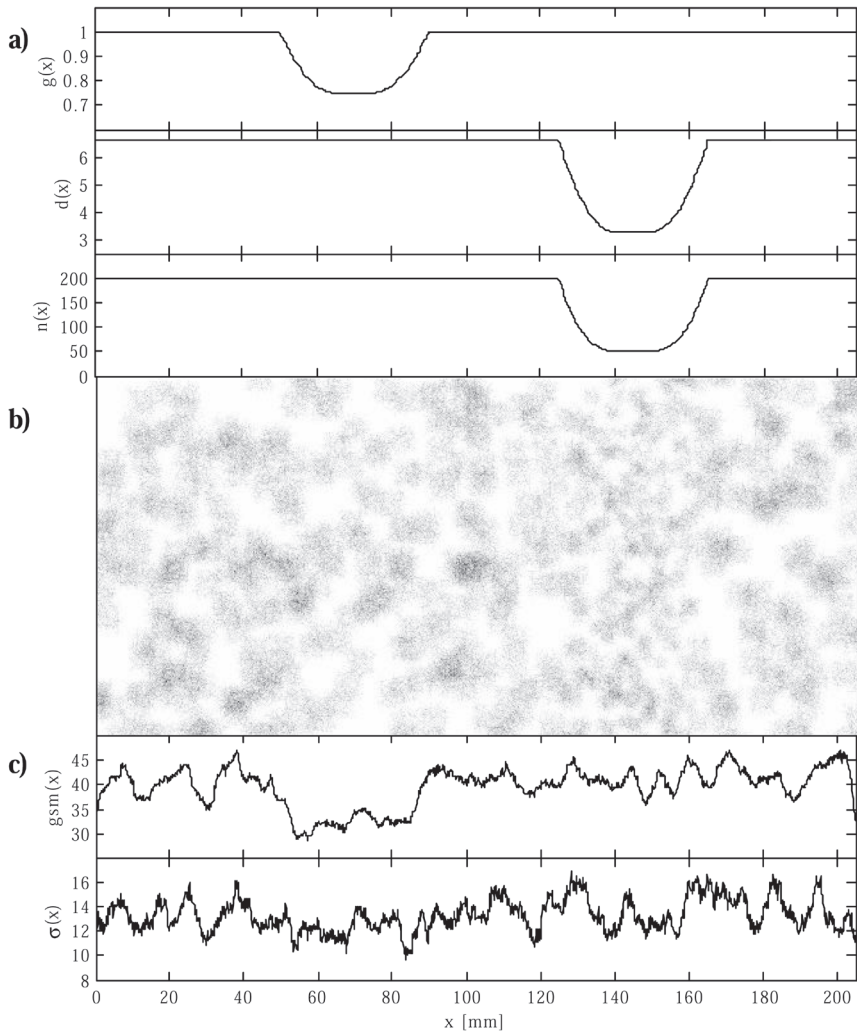


**Figure 4** Generation of streaks a) The target profiles for relative grammage  $g(x)$  [dimensionless], floc diameter  $d(x)$  [mm], and number of fibers per floc [dimensionless] control the size and number and density of flocs to be deposited randomly; b) An early ( $4 \text{ g/m}^2$ ) phase of floc deposition shows how different kinds of flocs start to aggregate at different CD positions; c) The mean grammage  $g_{sm}(x)$  [ $\text{g/m}^2$ ] and standard deviation  $\sigma(x)$  [ $\text{g/m}^2$ ] profiles for the final basis weight map of mean grammage  $40 \text{ g/m}^2$ .

## VALIDATION OF THE THEORETICAL APPROACH USING SIMULATED STREAKS

Decomposing streaks into grammage and formation components In order to verify the usefulness of Equations 16 and 17 for decomposing C-LE maps into contributions from the mean grammage profile and the local stochastic scale variations, a set of simulations were performed. To achieve reasonable statistical certainty, a large number of samples were analyzed for each experimental point. Table 1 summarizes details of our simulations.

Figure 5 shows the analysis of simulated grammage maps having either a

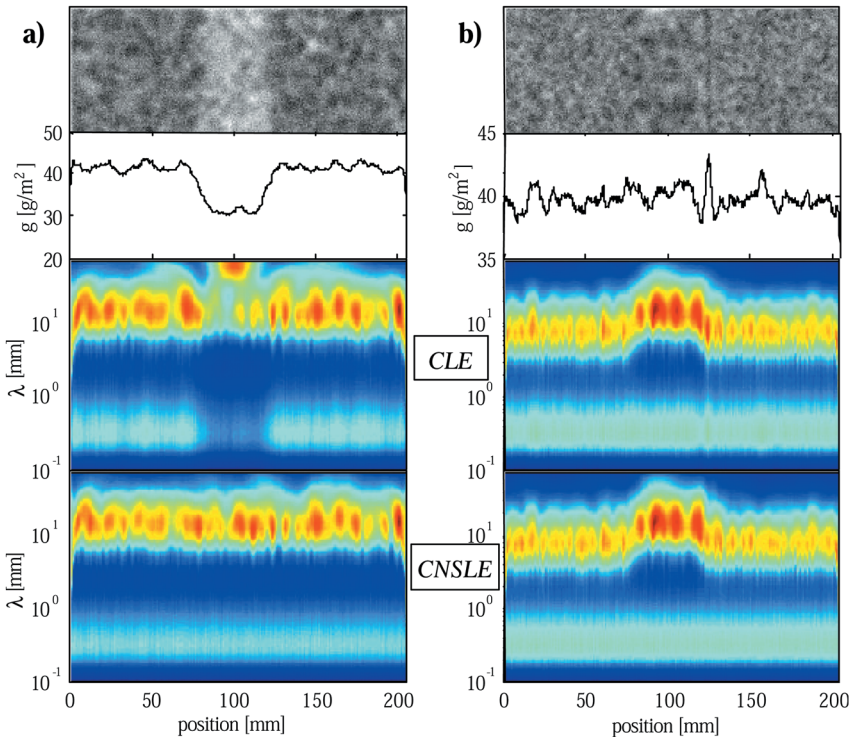


**Figure 5** a) Mean grammage streak; b) formation (floc size) streak. From top to bottom: *grammage map*; *mean grammage profile*; *composite local energy map*  $\langle \rho(a,b) \rangle dadb$ , cf. Eq. (6); and *composite normalized stochastic local energy map*  $\langle \rho_g^N(a,b) \rangle dadb$ , cf. Eq. (17). It is evident that the effect of mean grammage profile is effectively removed using CNSLE map without influencing energy distribution related to floc size variation.

grammage streak, cf. Figure 5a, or a floc size streak, cf. Figure 5b. The mean grammage was  $40 \text{ g/m}^2$  in both of these cases. The elementary flocs in this case had diameter of two fiber lengths, i.e.,  $d = 6.6 \text{ mm}$ . The basis weight of the grammage streak was 75% of the basis weight outside the streak. The 50 mm wide streak was positioned at the center ( $x = 102.4 \text{ mm}$ ), and is clearly visible in the grammage map shown in Figure 5a. The mean grammage profile of the data set, calculated from 10 samples is shown below the grammage map. The C-LE map of this data set, shown in the center, plots the scale as a function of position across the image. The effects of the grammage streak are clearly evident. A generally uniform spectral concentration, with peak at 110 mm, is disrupted in the center with a node in excess of 200 mm and a decrease in spectral density at finer scales. In the bottom Figure the CNS-LE map is shown. It is evident that any artifacts attributable to decreased grammage within the streak are absent, and the energy band is continuous through the position axis.

In the grammage map with the formation streak, shown in Figure 5b, the streak is much less apparent. Upon close inspection, one may notice coarser, “cloudier” flocs in the center, bracketed by finer flocs on either side. This image has a relatively flat grammage profile. In the C-LE map there is a shift of energy from lower wave-lengths to higher wavelengths. However, this type of streak does not influence the wavelengths between 0.1 mm and 1 mm. The CNS-LE map for the formation streak looks identical to the C-LE map. There only occurs a removal of energies related to small local mean grammage peak located at  $x \approx 125 \text{ mm}$ . These two examples clearly demonstrate that the CNS-LE map has the ability of negating effects resulting from a non-uniform mean grammage profile.

To explore this hypothesis under more demanding situations, we simulated, within the same image, overlapping mean grammage and floc size streaks, as shown in Figure 6. The target profiles of grammage,  $g(x)$ , and floc diameter  $d(x)$ , respectively, are shown in the top graph of that figure. Zones 1 through 9 identify positions where the streaks exist individually, where they are combined, and where transitions occur. The grammage map directly below reflects the intent of the applied profiles. At first glance, it is difficult to see the two different, overlapping streaks. However, the effect of the formation streak, in the form of cloudier, more diffuse flocs may be seen to the immediate right of the darker grammage streak. The C-LE map shown just below the grammage map has an interesting pattern, where the effects of the streaks on the spectral energy are evident, but not easily interpreted. To determine the validity of Equation 16 we separated the C-LE map into the static component, shown as the SMP-LE map in Figure 6b, and the stochastic component as the CS-LE map in Figure 6c. For the static component, (Figure 6b) the

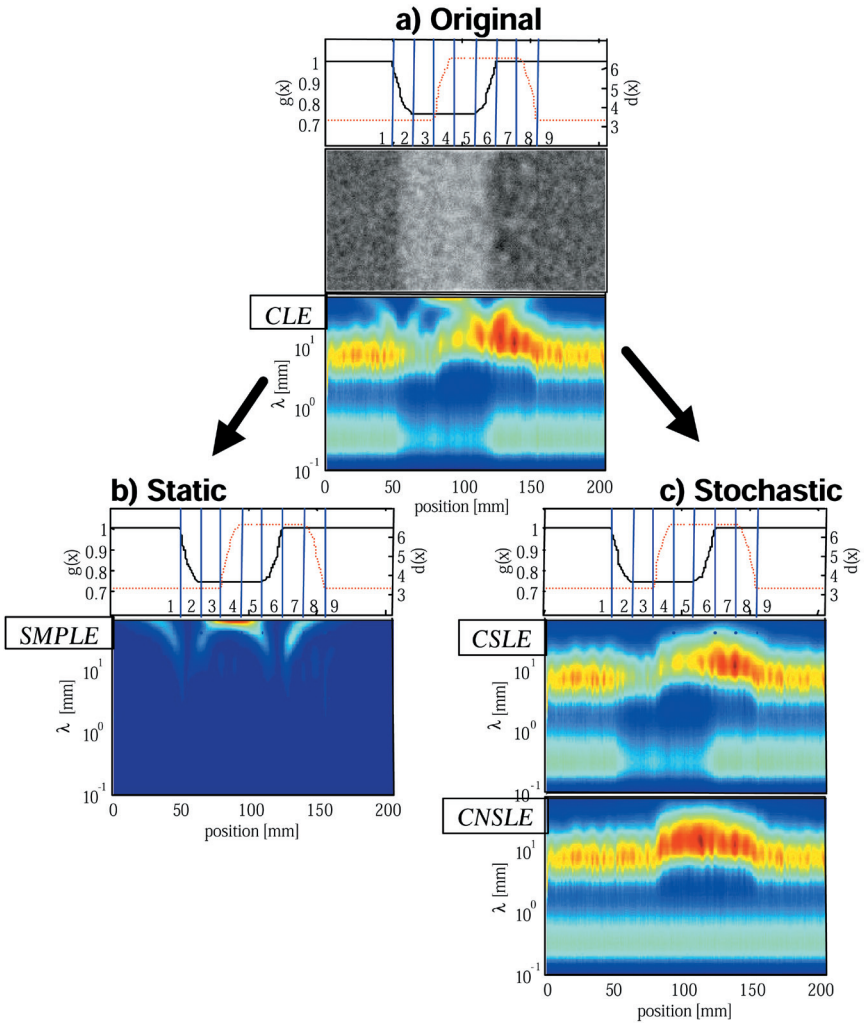


**Figure 6** Overlapping grammage and formation streaks. a) From top to bottom: target grammage profile (solid line), floc diameter profile (dotted line); *grammage* map and *composite local energy* map  $\langle \rho(a,b) \rangle dadb$ ; b) Static Component, target profiles and *static mean profile local energy* map  $\rho_s(a,b) dadb$ ; c) Stochastic Component, target profiles, *composite stochastic local energy* map  $\langle \rho_g(a,b) \rangle dadb$ , and *composite normalized local energy* map  $\langle \rho_g^N(a,b) \rangle dadb$ .

long-wavelength energy band defines the boundaries of the grammage streak occupying zones 2 through 6. For the stochastic component (Figure 6c), the intermediate CS-LE spectrum (top) and the more useful normalized CNS-LE map (bottom) are shown. The latter energy map shows the influence of the formation streak, with the effects of the grammage streak removed. A comparison of the lowest Static and Stochastic spectral plots reveals that a clean separation of the spectral responses of the two types of streaks was successfully achieved. Furthermore, the wavelength values for the spectral peaks, which is representative of the floc size distribution contained within the streaks as a function of position, was determined. This allows us to easily analyze structural scale variation *independent* of the mean grammage profile. This analytical tool may be used to determine the origin of statistically non-stationary variation features in papers and boards.

## **RESULTS FOR ANALYSIS OF PAPERS WITH STREAKS**

Examples of the application of the described analytical method, based on wavelet theory, are given by the analysis of laboratory and machine made papers that are known to have unidirectional non-uniformity in grammage and/or formation. Although the intensity of the defects exceeds generally accepted quality limits, the scale of the flocs, and the magnitude of the variance reasonably reflect results that can be expected in an assessment conducted under real circumstances.

### **Laboratory Handsheet**

Figure 7 shows the results for the analysis of a hand sheet prepared with a center region that is higher in grammage and has been allowed to flocculate. Thus we would expect both the static and stochastic components to represent these differences. The directionality of the non-uniformity is clearly evident in the grammage map at the top. However, while it may be possible to perceive differences in floc scale, and the contrast difference associated with increased grammage variation within the streak, with existing formation analytical methods, it is quite unlikely that a quantification of these two would be possible. The spectral plot shown directly below the mean grammage profile is the SMP-LE map indicating the grammage intensity. Both plots show the pattern of increased grammage, from which the dimensions can be easily obtained. The spectral plot shown at the bottom is the CNS-LE map of the stochastic component. In this plot, there are intense peaks in the center which result from the sensitivity to the discrete features in the grammage map. While

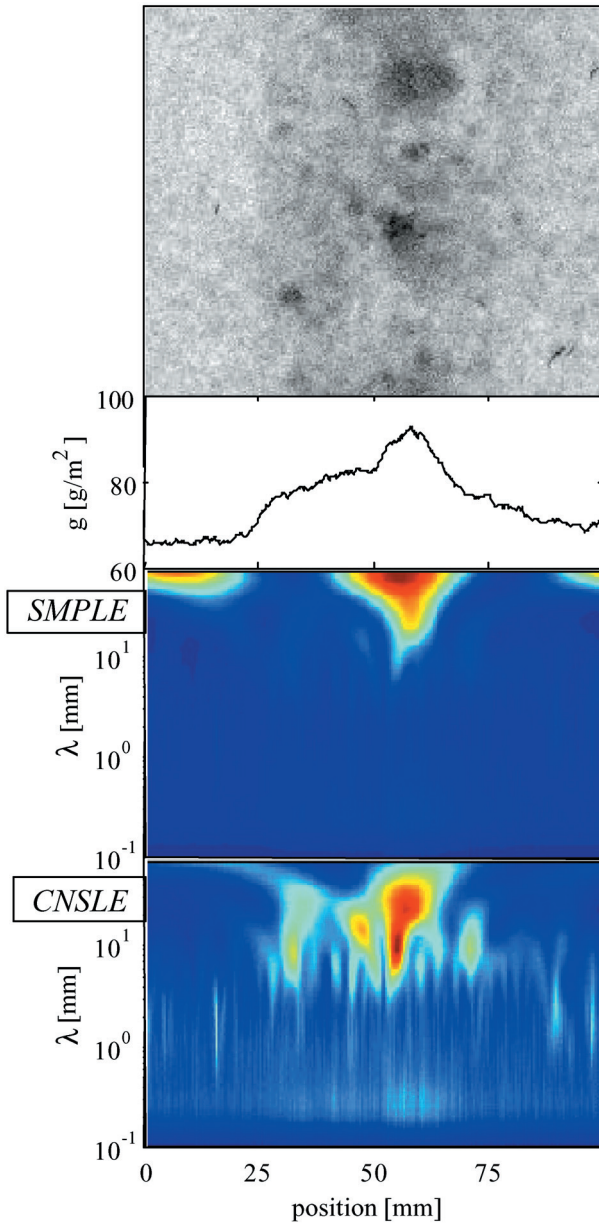


**Figure 7** Streaked Handsheet sample a) Grammage Map and b) Apparent Density Map. From top to bottom: maps, mean CD profile, Static Component, *static mean profile local energy map*, Stochastic Component, *composite normalized local energy map*.

the size of these features can be determined, clear imaging of the change in floc size is overwhelmed. On closer inspection, a subtle arc can be seen, rising from lower values at the edges to higher values in the center, which is an indication of the true variation in floc scale. Domination of these plots by individual features, as in this example, is a consequence of insufficient sample size to negate the effects of such features. An example of adequate sampling is given for the machine made paper.

### **Pilot Machine Made Paper**

Figure 8 shows the results obtained from the analysis of paper made on a pilot machine, where streaks were present. A larger area was tested as compared to the handsheet above. As can be seen in the grammage map, the streaks are well formed and relatively stable (within the sampling region). The machine direction is oriented vertically. The mean grammage profile and C-LE map directly below, show a pattern which suggests two principal wavelengths of flocs. Three streaks with wavelengths of about 50 mm are visible, and represent a static. In the mean grammage profile, variance about the streak sawtooth pattern is also apparent. The C-LE map quantifies the mean size of these two patterns, which can be seen as the row of circular peaks, and the ridge of elongated peaks centered at about 2–3 mm. While individual features are apparent, their size does not dominate the image, as was the situation with the laboratory sheet discussed above. Thus, the general structural differences will more clearly be visible in the spectral plots. This is also a nice demonstration of the need to have sufficient sampling in order to conduct a proper analysis.

The two lower spectral plots show the isolated static component, SMP-LE map (left) and the stochastic component, CNS-LE map. A clean separation of the two components was achieved. The SMP-LE map shows the energy related to the wavy character of the grammage variation. A subtle decrease in wavelength and intensity of the streaks, from image left to right, may be seen. The CNS-LE map has also a very rich structure of its own where the floc structure (formation) of the paper can be seen as the ridge of spectral peaks with  $\lambda$  intercept of about 2–3 mm. It also shows, for example, that at positions 50–75 mm the mean floc size is decreased independent of the local grammage profile, while floc intensity increases toward the right side of the image.

A different pilot machine sample was analyzed by applying the wavelet theory and comparing grammage and apparent density maps. Figure 9 shows the results for a) grammage, and b) apparent density. The sampling region is smaller (50 mm) than what was shown in Figure 8 (200 mm). For the grammage map, the mean grammage profile, and the static component and

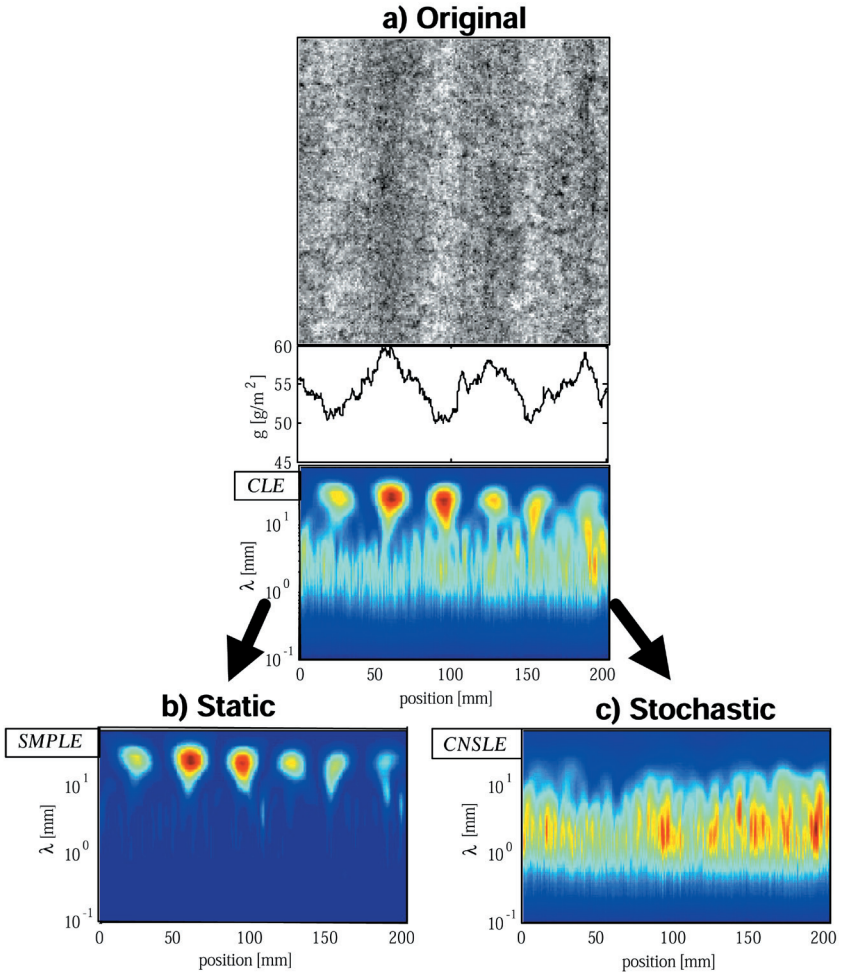


**Figure 8** A paper sample from a pilot machine test run. streaks. a) From top to bottom: *grammage* map, *floc diameter profile*, *composite local energy* map; b) *Static Component*, *static mean profile local energy* map; c) *Stochastic Component*, *composite normalized local energy* map.

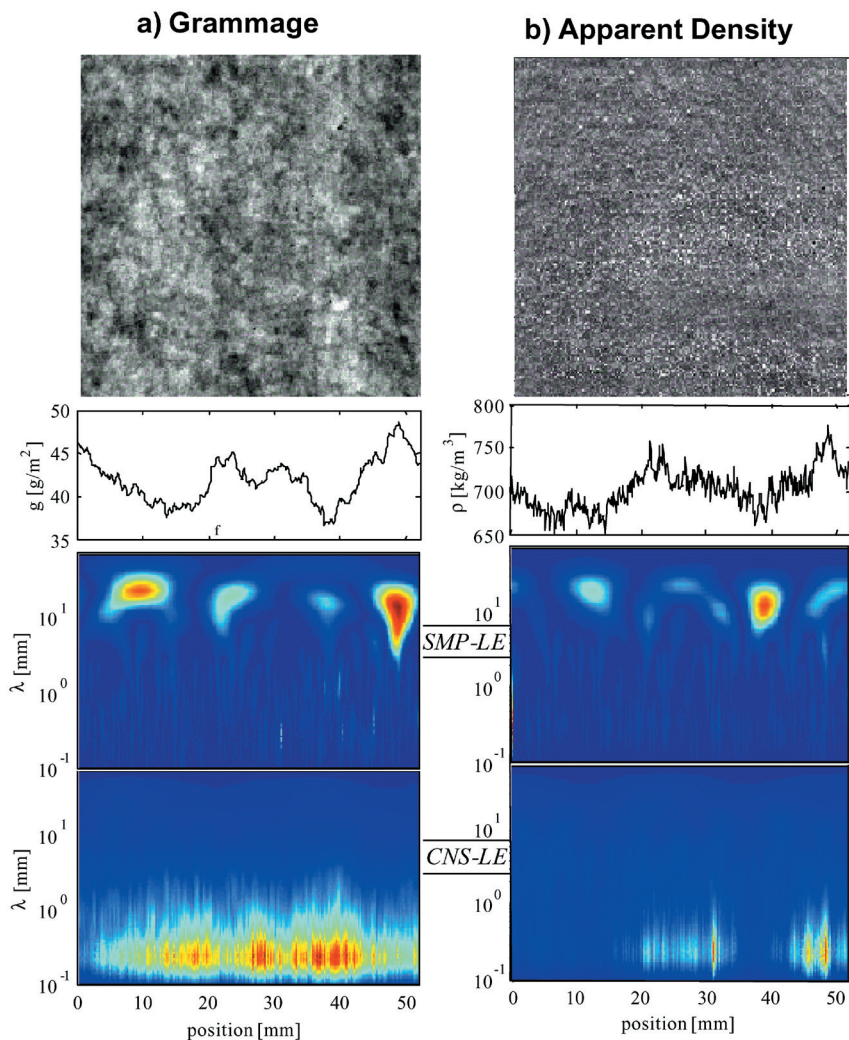


**Figure 9** Pilot machine sample a) Grammage Map and B) Apparent Density Map. From top to bottom: maps, mean CD profile, Static Component, *static mean profile local energy map*, Stochastic Component, *composite normalized local energy map*.

stochastic component maps (Figure 9 from top to bottom), the results are much the same as discussed above. The large-scale streak artifacts are isolated in the SMP-LE map, and the underlying formation structure is illustrated in the CNS-LE map.

Figure 10 shows the thickness map and the mean thickness values, as determined using the twin laser system. This thickness map was used to determine the apparent density map shown in Figure 9b. Figure 10 also provides a representation of the out of plane deformation that was determined for this sample. Note the ridge that exists at the 40 mm position. This was visible to the unaided eye.

The map shown in Figure 9b suggests a relatively uniform apparent density. Since this paper was uncalendered, this would be expected. Several of the large-scale features are visible in the SMP-LE map. Again, the limited sample set may make this data more subject to influence by individual features. The subtle differences between the peak locations cannot be attributed to actual differences in the structure. However, the stochastic component (CNS-LE), shown in the bottom spectral plot, shows spatial variation in apparent density. Two large clusters, centered at 27 mm and 47 mm are apparent. Since there does not appear to be a correlation with the grammage map results, the differences must be due to differences in the internal structure.

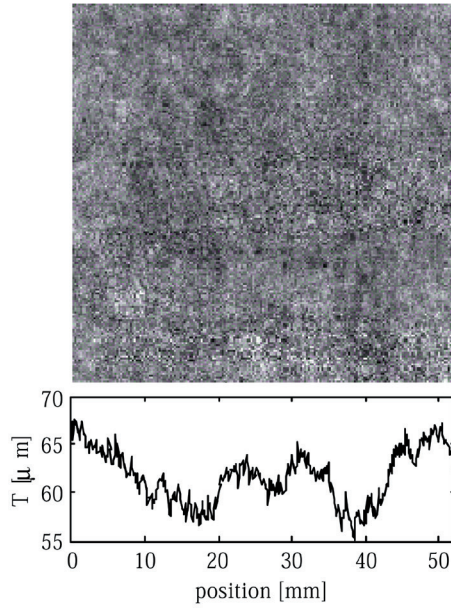
## CONCLUSIONS

A novel method for distinguishing between static and stochastic features in paper variability data was presented. The method made use of the spectral-spatial energy maps generated using a discrete implementation of a continuous wavelet transform of one dimensional series contained within the sample array. The theoretical basis for this method was presented.

In order to validate the method, simulated mass formation images containing streaks with different mean grammage or mean floc size, or combinations of the two. The method could clearly distinguish between the two types of streaks, and provided quantitative information about mean grammage values, floc size distribution, intensity of variance and the positions where any transition was occurring.

To demonstrate the application of this method, laboratory handsheets were prepared with different types of streaks within the sample. After imaging using  $\beta$ -radiographic imaging using storage phosphor detection system, samples were analyzed. While both the static and stochastic components were present, the large feature size tended to interfere with the wavelet transform analysis since individual features dominated the results.

### a) Thickness



### b) Out of Plane Deformation

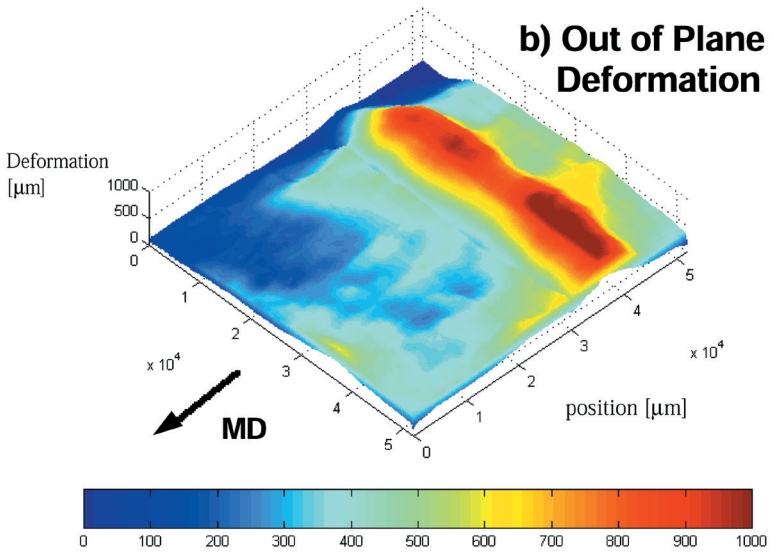


**Figure 10** Pilot machine sample; a) Local Thickness Distribution and Mean CD Profile; b) Out of Plane Deformation.

Pilot machine made papers that showed streaking were also analyzed for mass formation and local apparent density. The sample size was larger which improved the results obtained from wavelet analysis. The nodes of streaks, which were static in nature, were quite evident and the wavelength was easily determined from spectral density using wavelet analysis. The floc size distribution of the mass formation, independent of streaks, was also easily visible on inspection of the spectral plots, especially the manner in which the size changed as a function of position.

The local apparent density was determined from mass formation imaging and thickness mapping. Both the static and stochastic components of density appeared independent of the streaks in the pilot samples. However, anomalies that were oriented perpendicular to the streak did appear in density maps. These appeared as a slight density increase that was associated with an out of plane deformation.

## ACKNOWLEDGEMENTS

The support of the Empire State Paper Research Associates (E.S.P.R.A.), AES Engineered Systems and International Paper is greatly appreciated. We would also like to thank P. Jetsu of Metso Paper Corp. for supplying samples, and D. Haggart for construction of the laser thickness tester. Dr. Kellomäki expresses his appreciation of VTT Energy and TEKES for supporting his effort.

## REFERENCES

1. Norman, B. and Wahren, D., "Mass Distribution And Sheet Properties Of Paper," in Proc. 1973 Fundamental Properties of Paper Related to its Uses, Trans. Symp., Br. Pap. Board Ind. Fed., Cambridge: London, p. 7-73 (1973).
2. Madsen, V.H. and Aneliunas, A.E., "The effect of formation on print quality," *Tappi J.*, **51**( 7): 309-314 (1968).
3. Kajanto, I.M., "The effect of formation on print quality with woodfree offset papers," *Nordic Pulp Pap. Res. J.* **4**(1): 8-15 (1989).
4. Kajanto, I.M., "The effect of formation on absolute print unevenness in offset printing," *Paperi ja Puu*, **72**(6): 600-610 (1990).
5. Bernié, J.P. and Douglas, W.J.M., "Exploration of the print quality - paper formation relation," in Proc. 1997 Process & Product Quality Conference and trade Fair: Tappi Press, Atlanta, p. 73-77 (1997).
6. Matsubayashi, H., Takagishi, Y., Kataoka, Y., Saito, Y. and Miyamoto, K., "Influence of Coating Structure on Paper Quality," in Proc. 1992 TAPPI Coating Conference, Orlando, FL, Tappi Press, Atlanta, p. 161-172 (1992).

7. Leskela, M. and Luner, P., "Effect of formation on the optical properties of paper: A simulation," *Paperi Ja Puu*, **76**(4): 251–255 (1994).
8. Jordan, B.D., "Predicting the effect of formation on opacity and scattering coefficient," *J. Pulp and Paper Sci.*, **11**(2): J56–J59 (1985).
9. Mohlin, U.-B., "Fiber dimensions – formation and strength," in Proc. 2000 Progress in Paper Physics, A Seminar, Grenoble, FR, p. 5–14 (2000).
10. Deng, M. and Dodson, C.J.T., *Paper: An Engineered Stochastic Structure*, Tappi Press, Atlanta (1994)
11. Kerekes, R.J. and Schekk, C.J., "Effects of fiber length and coarseness on pulp flocculation," *Tappi J.*, **78**(2): 133–139 (1995).
12. Kiviranta, A., "Fiber and forming-related mechanisms affecting formation," in Proc. 1996 Tappi Papermakers Conference, p. 239–245 (1996).
13. Waterhouse, J.F., "Effect of papermaking variables on formation," *Tappi J.*, **76**(9): 129–134 (1993).
14. Egelhof, D. and Bubik, A., "Der Einfluss des Maschinenbaus auf die Blattbildung," *Wochenblatt für Papierfabrikation*, **122**(4): 111–117 (1994).
15. Chatterjee, A. and Dodson, C.T.J., *Role of Retention Aids in the forming process and on formation*, Univ. of Toronto. p. 57 (1993).
16. Farrington, T.E., "Soft X-Ray Imaging Can Be Used To Assess Sheet Formation And Quality," *Tappi J.*, **71**(5): 140–144 (1988).
17. Tomimasu, H., Kim, D., Suk, M. and Luner, P., "Comparison of four paper imaging techniques:  $\beta$ -radiography, electrography, light transmission, and soft X-radiography," *Tappi J.*, **74**(7): 165–176 (1991).
18. Cresson, T.M., Tomimasu, H. and Luner, P., "Characterization Of Paper Formation Part I: Sensing Paper Formation," *Tappi J.*, **73**(7): 153–159 (1990).
19. Norman, B. and Wahren, D., "The measurement of mass distribution in paper sheets using a beta radiographic method," *Svensk Papperstidning*, **77**(11): 397–406 (1974).
20. Dodson, C.T.J., "A Universal Law of Formation," *J. Pulp Paper Sci.*, **15**(4): J136–137 (1990).
21. Bernié, J.P. and Douglas, W.J.M., "Local grammage distribution and formation of paper by light transmission image analysis," *Tappi J.*, **79**(1): 193–202 (1996).
22. Jordan, B.D. and Nguyen, N.G., "Specific perimeter – a graininess parameter for formation and print-mottle textures," *Paperi ja Puu*, **6**(7): 476–482 (1986).
23. Norman, B. and Wahren, D., "A comprehensive method for the description of mass distribution in sheets and flocculation and turbulence in suspensions," *Svensk Papperstidning*, **75**(20): 807–818 (1972).
24. Dodson, C.T.J., "Spatial variability and the theory of sampling in random fibrous networks," *J. Roy. Statist. Soc. B*, **33**(1): 88–94 (1971).
25. Niskanen, K., Nilsen, N., Hellen, E. and Alava, M., "KCL-PAKKA: Simulation of the 3D structure of paper," in Proc. 1997 The Fundamentals of Papermaking: 11th Fundamental Research Symposium, Cambridge, UK: Pira International, p. 1273–1291 (1997).
26. Brendemuehl, R.C. and Borchert, J.E., "Real-time spectral analysis of machine directional basis weight variations in paper," *Tappi J.*, **59**(8): 79–81 (1976).

27. Parker, I.H., "Frequency analysis in the paper industry," *Appita*, **28**(6): 409–413 (1975).
28. Holik, H., HeB, H., Tietz, M. and Drtina, P., "Fluid Mechanics in the Headbox – The Key to Improving Paper Quality," in Proc. 1994 TAPPI Engineering Conference: TAPPI Press, Atlanta, p. 247 (1994).
29. Boulay, R., Drouin, B. and Gagnon, R., "Measurement of Local Fibre Orientation Variations," *J. Pulp and Paper Sci.*, **12**(6): J177–J181 (1986).
30. Soremark, C., Johansson, G., and Kiviranta, A., "Characterization and elimination of fiber orientation streaks," in Proc. 1994 Tappi Engineering Conference, p. 97–104 (1994).
31. Furst, T., "A new instrument capable of measuring cross machine profiles of internal bond strength," in Proc. 1999 27th EUCEPA conference – Crossing the millennium frontier, emerging technical and scientific challenges, Grenoble, FR, p. 287–292 (1999).
32. Griffin, J., Eschbach, P., Sturm, S. and Pfeifer, R., "A new concept for 100% measurement of paper basis weight," in Proc. 1998 Process & Product Quality Conference, Tappi Press, Atlanta, p. 143–149 (1998).
33. Perento, J. and Erho, T., "New tools for the papermaker to improve the printability of paper," *Paper Tech.*, **40**(9): 29–34 (1999).
34. Keller, D.S., Lewalle, J. and Luner, P., "The Analysis of Paper Variability Using The Wavelet Transform," *Paperi ja Pu*, **81**(6): 440–446 (1999).
35. Keller, D.S., Lewalle, J. and Luner, P., "Wavelet Analysis of Simulated Paper Formation," *Paperi ja Pu*, **81**(7): 499–505 (1999).
36. Bouydaïn, M., Colom, J. and Pladellorens, J., "Using wavelets to determine paper formation by light transmission image analysis," *Tappi J.*, **82**(7): 153–158 (1999).
37. Mallet, G., "A Theory for multiresolution signal decomposition: The wavelet representation," *IEEE Trans. Pattern Anal. and Machine Intell.*, **11**(7): 674 (1989).
38. Johansson, P. -A., "Evaluation of grey-tone evenness using bandpass-filtering on a video-scanning image -analyzer," in Proc. 1983 3rd Scandanavian Conference on Image Analysis, Studentlitteratur, Lund, p. 188–193 (1983).
39. MacGregor, M. A., Johansson, P.-Å., and Béland, M.-C., "Measurement of small-scale gloss variation in printed paper," in Proc. 1994 Proceedings International Printing and Graphics Arts Conference, Tappi Press, Atlanta, p. 33–43 (1994).
40. Sara, H., "The Characterization and Measurement of Paper Formation with Standard Deviation and Power Spectrum", Helsinki University of Technology, (1978).
41. Komppa, A. and Ebeling, K., "Correlation Between The Areal Mass And Optical Densities In Paper," in Proc. 1983 Role Of Fundam. Res. In Pmkg. Trans. BPBIF Symp., Cambridge: Mechanical Engineering Publications, p. 603–633 London, (1983).
42. Steffner, O., Nylund, T. and Rigdahl, M., "Influence of the calendering conditions on the structure and the properties of woodfree paper – a comparison between soft nip calendering and hard nip calendering," *Nordic Pulp And Paper Res. J.*, **13**(1): 68–75 (1998).

43. Kimura, M., Matsui, S. and Nakato, K., "Method for obtaining a local density variation in a sheet," *J. Soc. Fiber Sci. Technol. Japan*, **41**(7): T308–312 (1985).
44. Fellers, C., Andersson, H., and Hollmark, H., in *Paper Structure and Properties*, J. A. Bristow and P. Kolseth, Editors, Marcel Dekker, New York. p. 151 (1986).
45. Schultz-Eklund, O., Fellers, C. and Johansson, P., "Method for the local determination of the thickness and density of paper," *Nordic Pulp And Paper Res. J.*, **(3)**: 133–154 (1992).
46. Wagberg, P. and Johansson, P., "Surface profilometry – comparison between optical and mechanical sensing on printing papers," *Tappi J.*, **76**(12): 115–121 (1993).
47. Elgay, P., Non-contact laser surface profilometry, M. S. Thesis, SUNY College of ESF (1994).
48. Oba, Y., Z Directional Structural Development and Density Variation, Ph. D. Thesis, University of Manchester Institute of Science and Technology (1999).
49. Izumi, H. and Yoshida, Y., "Development and application of a system for determining paper non-uniformity," in Proc. 1999 Pulp and Paper Research Conference, Japan (1999).
50. I'Anson, S.J. and Kropholler, H.W., "Enhancing Visibility of Wire-Mark by Image Analysis," *J. Pulp Paper Sci.*, **17**(1): J22–26 (1991).
51. Praast, H. and Göttsching, L., "Detailed Analysis of Geometry and Intensity of Wire Marks," *Das Papier*, **44**(10): 529–537 (1990).
52. Norman, B., "The formation spectrum," *Tappi.*, **68**(7): 104–105 (1985).
53. Johansson, P. and Norman, B., "Methods For Evaluating Formation, Print Unevenness, And Gloss Variations Developed At STFI," in Proc. 1996 Tappi Process And Product Quality Conf., Cincinnati, OH, p. 139–145 (1996).
54. Foyn, B., Two Dimensional Directional Analysis of Paper Formation, University of Oslo (1991).
55. Kaiser, G., *A Friendly Guide to Wavelets*, Birkhauser, Boston (1994)
56. Farge, M., Hunt, J. C. R., Vassilicos, J. C., editors, *Wavelets, Fractals, and Fourier Transforms.*, Clarendon Press, Oxford (1993)
57. Farge, M., "Wavelet Transforms and Their Applications to Turbulence," *Annual Rev. Fluid Mech.*, **24**: 395–457 (1992).
58. Brasseur, J.G. and Wang, Q., "Structural evolution of intermittency and anisotropy at different scales analyzed using three dimensional wavelet transforms," *Phys. Fluids A*, **4**(11): 2538–2554 (1992).
59. Everson, R., Sirooich, L. and Sreenivasan, K.R., "Wavelet analysis of the turbulent jet," *Physics Letters A*, **145**: 314–322 (1990).
60. Liandrat, J. and Moret-Bailly, F., "The wavelet transform: some applications to the fluid dynamics and turbulence," *Eur. J. Mech. B/Fluids*, **9**: 1–19 (1990).
61. Zubair, L.M., Studies in Turbulence Using Wavelet Transforms for Data Compression and Scale Separation, Ph.D. Thesis, Yale University (1993).
62. Barabasi, A.-L. and Stanley, H.E., *Fractal Concepts in Surface Growth*, Cambridge University Press, Cambridge (1995)
63. Keller, D.S. and Pawlak, J.J., " $\beta$ -Radiographic Measurement Of Paper Formation Using A Storage Phosphor System," *J. Pulp And Paper Sci.*, **27**(4): (2001).

64. Ng, W.K. and Dodson, C.T.J., "Rapid Formation Performance Test," in Proc. 1995 Int. Paper Phys. Conf, Niagara-on-the-Lake, ON, Tappi Press, p. 49–59 (1995).

## Transcription of Discussion

# CHARACTERIZATION OF NON-STATIONARY STRUCTURAL NON-UNIFORMITIES IN PAPER

*Markku Kellomäki<sup>1</sup>, Joel P. Pawlak, Yong-Joo Sung and  
D. Steven Keller*

State University of New York College of Environmental Science and Forestry

<sup>1</sup>Permanent Address: VTT Energy, Finland

*Patrick Gane*      Omya AG

May I congratulate on picking up the concept of wavelet transforms in dealing with this problem. Some years ago when I was faced with looking at surface profile roughness and realising that there was a stochastic component, the way I tackled it was to abandon the Fourier transform and move to square wave functions and operate those over very short correlation lengths. Essentially what you have here is part of a wave which is over a short correlation length. You showed that in fact it is indeed something of a compromise because of the uncertainty principle, and when you came to describe your de-convolution between repeatable patterns and stochastic patterns you were able to cope with rather simple repeat patterns however I think that in many surfaces and paper surfaces there may be more complex repeat patterns rather than some of the simple ones you looked at such as the wire marks and the streaks. I wonder if it would be possible to combine the two techniques. One would be to use either Fourier or other wave transforms look at the decay of correlation of these continuous functions. The decay of correlation would be able to tell you which continuous functions had a long correlation on the surface and were therefore relevant to repeat patterns. These could in fact then be subtracted from the main image leaving you only the stochastic information which you could then deal with using your wavelet theory and perhaps then be able to de-convolute even more complex systems.

## *Discussion*

*Markku Kellomäki*

Yes, for example removing wire marks, many of us know it is very a difficult task. It has been tried many times through cosine transform to extract peaks and delete them and transform back to get only the stochastic data, but it has failed because the amplitude is not constant. The amplitude of the periodic function is not constant over the whole range, and I think wavelet transforms could help in that sense. Also there are many other local spectral analysing methods and we are now trying something that is very mathematical, that I am not familiar with – my co-worker is working on that. It is based on modelling with Gaussian functions the whole formation image and then from there deduce the local wire mark intensity.

*Patrick Gane*

Yes even if you were to consider a Gaussian distribution of the correlation lengths you could then use that for the criterion for subtraction of the Fourier transform leaving you free then to do your wavelets on the stochastic part.

*John Parker*      Consultant

I too would like to congratulate you on your presentation of the wavelet approach, but I must point out, in fairness to others that have used Fourier methods, that they could also have analysed the variations caused by streaks that are given as an example in this paper. It is necessary only to scan slowly across the width of a moving paper web and at intervals to measure the mean grammage and also to compute a spectrum of the MD grammage variation. A plot of this grammage would reveal streaks of heavy or light paper, while the shapes of the spectra would indicate the presence of streak where the flocs differed from the norm either in size or in intensity. More details of this approach may be found referenced in papers by Kenny Corscadden whose work was mentioned by M.H. Waller in the 5<sup>th</sup> session of the Symposium.

*Ramin Farnood*      University of Toronto

I have a comment regarding the simulated paper in which you used model flocs. I wanted to caution you that statistics of real paper would be substantially different from a structure made of single size flocs. That was demonstrated in 1995 in a paper that we published and in 1997, so in order to extract useful information from your simulation, you would need to consider the distribution of floc sizes which is in fact very easy to implement in the model that you have.

*Markku Kellomäki*

In this case we start the simplest way and of course it is trivial to introduce fibrel length distributions, fibre curl distributions, floc size distributions, all kinds of things to improve digital paper, but I still can see even in this case in which the elementary flocs were of the same size, they did have some random roughness around them thermo-period. In the wavelet domain there is some spread of energy, so there will be a further spread due to these distributions, but I think that it won't change, if you have enough data, the conclusions shown here.